Structural Basis for Inhibition of the Protein Tyrosine Phosphatase 1B by Phosphotyrosine Peptide Mimetics[†,‡]

Matthew R. Groves,[§] Zhu-Jun Yao,[||] Peter P. Roller,[||] Terrence R. Burke, Jr.,[||] and David Barford*[,§]

Laboratory of Molecular Biophysics, Department of Biochemistry, University of Oxford, South Parks Road, Oxford, OX1 3QU, United Kingdom, and Laboratory of Medicinal Chemistry, Division of Basic Sciences, National Cancer Institute, National Institutes of Health, Bethesda, Maryland 20892

Received July 15, 1998; Revised Manuscript Received October 23, 1998

ABSTRACT: Protein tyrosine phosphatases regulate diverse cellular processes and represent important targets for therapeutic intervention in a number of diseases. The crystal structures of protein tyrosine phosphatase 1B (PTP1B) in complex with small molecule inhibitors based upon two classes of phosphotyrosine mimetics, the (difluoronaphthylmethyl)phosphonic acids and the fluoromalonyl tyrosines, have been determined to resolutions greater than 2.3 Å. The fluoromalonyl tyrosine residue was incorporated within a cyclic hexapeptide modeled on an autophosphorylation site of the epidermal growth factor receptor. The structure of this inhibitor bound to PTP1B represents the first crystal structure of a non-phosphonate-containing inhibitor and reveals the mechanism of phosphotyrosine mimicry by the fluoromalonyl tyrosine residue and the nature of its interactions within the catalytic site of PTP1B. In contrast to complexes of PTP1B with phosphotyrosine-containing peptides, binding of the fluoromalonyl tyrosine residue to the catalytic site of PTP1B is not accompanied by closure of the catalytic site WPD loop. Structures of PTP1B in complex with the (difluoronaphthylmethyl)phosphonic acid derivatives reveal that substitutions of the naphthalene ring modulate the mode of inhibitor binding to the catalytic site and provide the potential for enhanced inhibitor affinity and the generation of PTP-specific inhibitors. These results provide a framework for the rational design of higher affinity and more specific phosphotyrosine mimetic inhibitors of not only protein tyrosine phosphatases but also SH2 and PTB domains.

Protein tyrosine phosphatases (PTPs)[1] play essential roles in the regulation of cellular processes, including growth, proliferation and differentiation, metabolism, the immune response, cell−cell adhesion, and cell−matrix contacts (*1*, *2*). The PTPs comprise a large and diverse family of enzymes comprising nontransmembrane cytosolic and receptor-like transmembrane forms. The catalytic domains of PTPs are highly conserved, consisting of ∼250 amino acids that are characterized by an 11-residue PTP signature motif, (I/V)-HCXAGXXR(S/T)G, containing the catalytically essential Cys and Arg residues. Diversity within the family is generated by the nature of the noncatalytic segments attached to the N- and C-termini of the catalytic domains, which provide regulatory and subcellular targeting functions (*1*−*3*). The C-terminal 35 amino acids of PTP1B, for example, are necessary and sufficient for targeting the enzyme to the cytosolic side of the endoplasmic reticulum (*4*), whereas the N-terminal SH2 domains of the SHPs, provide a mechanism for phosphotyrosine peptides to determine both the subcellular location and the catalytic activity of these enzymes (*1*, *5*, *6*). The extracellular segments of many receptor-type PTPs share structural features with cell adhesion molecules, including immunoglobulin domains and fibronectin-type III motifs, suggesting that these phosphatases may provide a direct link between cell−cell interactions and the level of cytosolic protein tyrosine phosphorylation. The dual specificity phosphatases and low molecular weight PTPs, despite the diversity of their tertiary structures, are related to the tyrosine-specific PTPs by virtue of the presence of the PTP signature motif and related catalytic mechanism (*3*).

The physiological importance of the PTPs has been demonstrated by numerous studies. Inactivating mutations within the SH2 domain containing PTP, SHP-1 are the basis for severe immune dysfunction that is characteristic of the moth-eaten murine phenotype (*7*). Recently, PTEN has been implicated as a product of a tumor suppressor gene (*8, 9*) that may play roles to regulate integrin-dependent cell migration (*10*). PTP1B has been implicated as an important component of the insulin signaling pathway, dephosphorylating the activated insulin receptor (*11*), and negatively regulating the pathway (*12*). The receptor-like PTP, CD45, is essential for initiating T cell and B cell receptor signaling

[†] This work was supported by a Framework IV grant from the European Union to D.B.

[‡] The atomic coordinates for the PTP1B-INH, PTP1B-TPI, and PTP1B-FOMT complexes have been deposited with the Brookhaven Data Bank (accession numbers: 1bzj, 1bzc, and 1bzh).

* Corresponding author. Tel: 44 1865 275377. Fax: 44 1865 275182. E-mail: davidb@biop.ox.ac.uk.

[§] University of Oxford.

[||] National Cancer Institute.

[1] Abbreviations: NAPTH, [1,1-difluoro-1-(naphth-2-yl)]methylphosphonic acid; INH, [1,1-difluoro-1-((6-carboxy)naphth-2-yl)]methylphosphonic acid; TPI, [1,1-difluoro-1-((6-carboxamidoglutamic)naphth-2-yl)]methylphosphonic acid; OMT, L-*O*-(2-malonyl)tyrosine; FOMT, 4′-*O*-[2-(2-fluoromalonyl)]-L-tyrosine; PTP, protein tyrosine phosphatase; pTyr, phosphotyrosine; rmsd, root-mean-square deviation.

10.1021/bi9816958 CCC: $15.00
Published on Web 12/08/1998

cascades; hence inhibitors of CD45 would be predicted to be potent and specific immunosuppressants. Because of the importance of PTPs in mediating signal transduction processes, the structure-based design of small molecule PTP inhibitors is currently of great importance (*13*). Such efforts are aided by the crystal structures of unliganded PTP1B (*14*) and of PTP1B complexed with a phosphotyrosine- (pTyr) containing hexapeptide based upon an autophosphoryation site of the epidermal growth factor receptor (Asp_{988}-Ala-Asp-Glu-pTyr-Leu_{993}) (*15*).

The crystal structure of the PTP1B−pTyr peptide complex revealed that the pTyr residue of the peptide is buried within a catalytic site pocket 11 Å in length (*15*). The base of the catalytic site is formed by residues of the PTP signature motif with the phosphate group of pTyr coordinated by main-chain amide groups of the PTP motif and the side chain of Arg 221, such that the phosphorus atom is situated adjacent to the nucleophilic sulfur of Cys 215. Three loops bearing invariant residues form the sides of the catalytic pocket and contribute to catalysis and substrate recognition. The binding of phosphopeptide by PTP1B is accompanied by a conformational change of one of these loops (the WPD loop), which comprises residues 179−187. This loop shifts by over 8 Å to close over the phenyl ring of the bound pTyr residue and allows the side chain of Asp 181 to act as a general acid in the catalytic mechanism. The side chain of Arg 221 reorients to optimize electrostatic interactions with the bound phosphate group. This shift is coupled to the motion of the WPD loop through the hydrogen bond between the guanidino NH1 group of Arg 221 and the carbonyl oxygen of Pro 180 as well as hydrophobic interactions between the aliphatic portion of Arg 221 and the side chain of Trp 179. A highly ordered water molecule forms hydrogen bonds to both the bound phosphate group, the amide nitrogen of Phe 182, and the amide side chain of Gln 266. These interactions, along with the hydrophobic packing of the side chain of Phe 182 onto the pTyr aromatic ring, stabilize the closed, catalytically competent conformation of the loop (*15*).

One approach to the development of PTP inhibitors is based upon nonhydrolyzable analogues of phosphotyrosine. Burke et al. demonstrated that the replacement of pTyr in the D-A-D-E-pY-L peptide with difluorophosphonomethyl phenylalanine resulted in an inhibitor with an IC_{50} of 100 nM toward PTP1B (*16*). Although this compound has a remarkable affinity for PTP1B, its in vivo use would be limited owing to its large size and high charge complement that reduces cell membrane permeability. Subsequent experiments demonstrated that arylmethyl difluorophosphonates, lacking the peptide component, retained inhibitory potency (*17*). The addition of a second aryl ring yielding (difluoronaphthylmethyl) phosphonate resulted in a significant increase in potency (K_i = 179 μM) (NAPTH, Figure 1). The crystal structure of this inhibitor complexed with PTP1B (*18*) revealed that the molecule binds to the catalytic site with the WPD loop in the closed conformation, reminiscent of the PTP1B−pTyr complex structure (*15*). The *Pro-S* fluorine atom of the inhibitor accepts a hydrogen bond from the amide nitrogen of Phe 182, replacing the catalytic site water molecule. The structure also indicated that addition of a hydroxyl to the naphthyl 4-position (D, Figure 1) could mimic a water molecule found in the complex, allowing additional hydrogen bonds to Tyr 46 and Lys 120. This compound displays a much increased affinity toward PTP1B, with a K_i of 90 μM (*18*). Functional substitution of the naphthalene ring with groups mimicking the peptidic main chain have led to enhanced PTP1B−inhibitor affinity (for example INH and TPI, Figure 1).

More recently, a new non-phosphorus-containing pTyr mimetic, L-*O*-(2-malonyl)tyrosine (OMT), was demonstrated to inhibit both PTPs and SH2 domains with significant potency when incorporated into peptides. For example, an OMT-containing peptide (D-A-D-E-OMT-L) inhibits PTP1B with an K_i of 13 μM (Figure 1) (*20*). By incorporation of this phosphotyrosine mimetic into a cyclic hexapeptide modeled on the D-A-D-E-pY-L sequence, an 18-fold enhancement in potency was obtained (*20*). Replacement of the OMT residue in this cyclic peptide with the fluorine-containing OMT analogue, (*4′-O*-[2-(2-fluoromalonyl)]-L-tyrosine) "FOMT" (*21*) has resulted in even greater potency (*22*) (Figure 1). Prodrug protection of the malonyl group as its carboxylic acid diester could potentially increase cellular penetration and overcome problems of bioavailability characteristic of the phosphonate-based pTyr mimetics.

For understanding the structural basis for protein−inhibitor specificity and for rational improvement of protein−inhibitor affinities, the structures of a number of protein−inhibitor complexes are required. Here, we describe the crystal structure of a complex of PTP1B with the FOMT peptide inhibitor. This structure reveals the basis for the mimicry of the phosphotyrosine−PTP1B interactions by the malonyltyrosine residue. We also describe the crystal structures of complexes of PTP1B with derivatives of [1,1-difluoro-1-(naphth-2-yl)]methylphosphonic acid (NAPTH, Figure 1), one of which, TPI (Figure 1), contains a carboxamidoglutamic acid group designed to mimic a peptide moiety. These latter derivatives display enhanced affinity for PTP1B (*23*), and the crystal structures provide an explanation for these properties. Analysis of these PTP1B−inhibitor interactions can reasonably be expected to stimulate a further round of rational drug design, developing compounds with higher affinity and selectivity.

EXPERIMENTAL PROCEDURES

Preparation of Materials. Human PTP1B (residues 2−298) was purified as described previously (*24*). The cyclic peptide cyclo[CH_2CO-D-A-D-E-(L-FOMT)-L-Cys] was synthesized according to methodologies used for the preparation of its L-OMT analogue (*20*). Synthesis of (difluoronaphthylmethyl) phosphonic acids, INH and TPI, has been reported (*23*).

Crystallization of PTP1B Catalytic Domain with Inhibitors. PTP1B−[1,1-difluoro-1-((6-carboxy)naphth-2-yl)]-methylphosphonic acid (INH) (Figure 1) complex crystals were prepared by soaking crystals of the catalytic site Cys 215 to Ser mutant of PTP1B in a solution containing 20 mM INH, 0.1 M Hepes (pH 7.5), 0.2 M magnesium acetate, 16% (w/v) PEG 8000, and 15% (v/v) 2-methyl-2,4-pentanediol (MPD) for 1 h. The PTP1B−TPI complex crystals were prepared by cocrystallizing 5 mM TPI with 10 mg/mL of PTP1B using the wild-type PTP1B crystallization conditions (*24*). PTP1B−FOMT peptide inhibitor complex cocrystals were obtained by cocrystallizing 5 mM FOMT with 10 mg/mL of wild-type PTP1B using conditions similar to those of native PTP1B crystals, namely, 16% (w/v) PEG 4000,

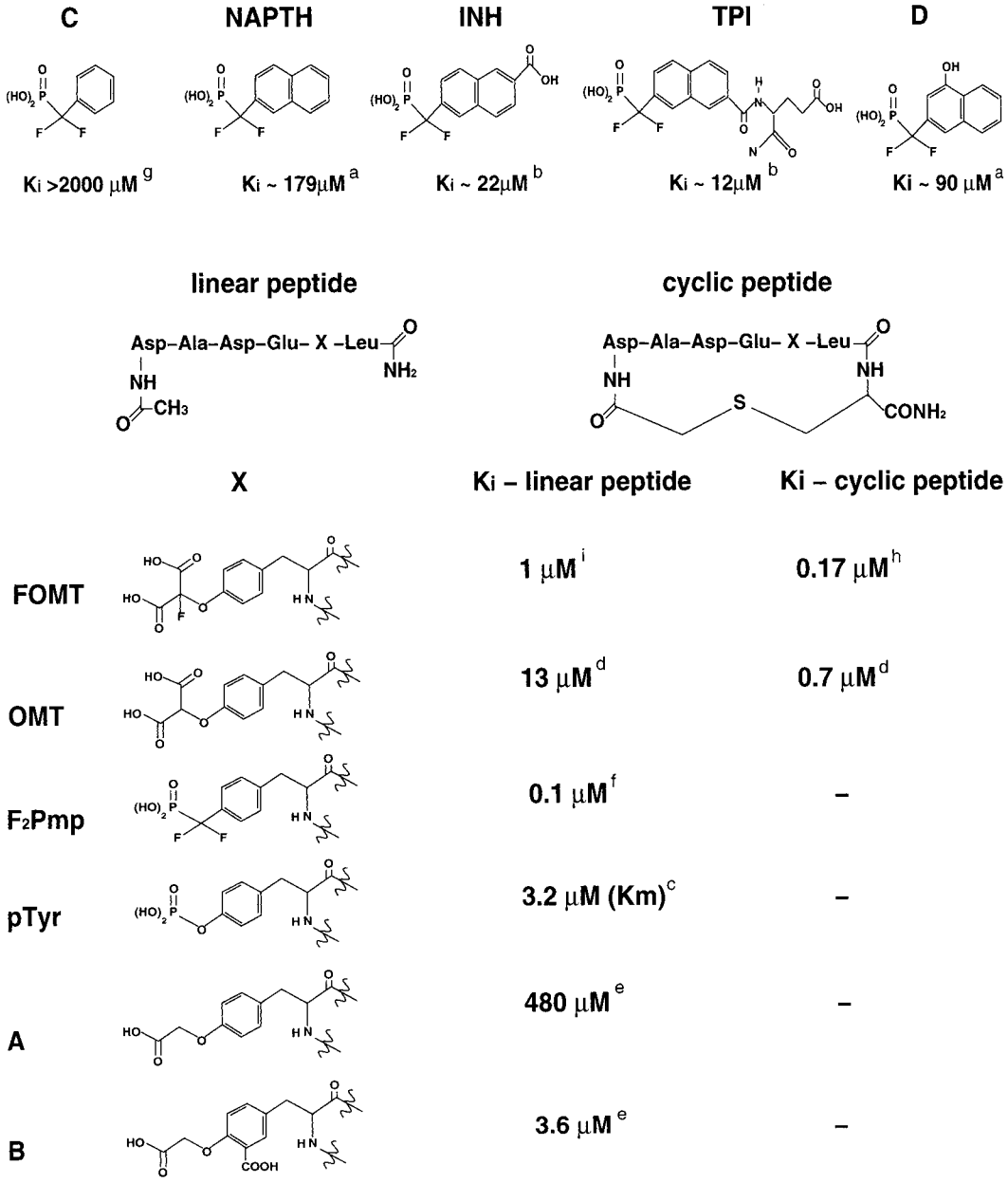

FIGURE 1: Chemical structures of PTP1B inhibitors used in this study and related inhibitors and their K_i toward PTP1B. Footnotes: a, ref *18*; b, ref *23*; c, ref *36*; d, ref *20*; e, ref *37*; f, ref *16*; g, ref *17*; h, ref *22*; i, ref *21*. Abbreviations: NAPTH, [1,1-difluoro-1-(naphth-2-yl)]-methylphosphonic acid; INH, [1,1-difluoro-1-((6-carboxy)naphth-2-yl)]methylphosphonic acid; TPI, [1,1-difluoro-1-((6-carboxamidoglutamic)-naphth-2-yl)]methylphosphonic acid; OMT, L-*O*-(2-malonyl)tyrosine; FOMT, 4′-*O*-[2-(2-fluoromalonyl)]-L-tyrosine.

0.2 M magnesium chloride, and 0.1 M Hepes (pH 8.0) using the hanging drop vapor diffusion method at 4 °C.

Data Collection and Processing. Data from the PTP1B−INH and PTP1B−TPI inhibitor complex crystals were collected using a Rigaku rotating anode source on a 30 cm MAR research scanner. Data from PTP1B−FOMT peptide inhibitor complex crystals were collected at station 5.2R the ELETTRA synchrotron light source, Trieste, Italy. Inhibitor complex crystals were prepared for data collection by incubation in a cryoprotectant buffer consisting of the crystallization buffer, 15% (v/v) MPD, and the appropriate inhibitor (20 mM INH, 5 mM TPI, and FOMT), transferred to a loop and flash-frozen in a stream of nitrogen gas at 100 K. Data were processed using the HKL package (*25*).

Structure Determination of the PTP1B Inhibitor Complexes. PTP1B−INH Complex. The starting model for this structure was the previously determined PTP1B-[1,1-difluoro-1-(naphth-2-yl)]methylphosphonic (NAPTH) inhibitor complex (*18*). The atomic model was refined with X-PLOR (*26*) using a simulated annealing approach with coordinates for the inhibitor omitted from the initial refinement procedure. The simulated annealing omit map revealed clear electron density for the inhibitor bound to the catalytic site with density attributable to the carboxylate group attached to the naphthyl 6-position (Figure 2). Further atomic and restrained *B* factor refinement with inclusion of the inhibitor coordinates resulted in an *R* factor of 0.208 for data to 2.25 Å resolution (Table 1).

PTP1B−TPI Complex. For determination of the PTP1B−TPI complex, the unliganded native PTP1B coordinates were used as a search model for molecular replacement using AMORE (*27*). Initial density in a difference Fourier map was sufficient to place the TPI inhibitor unambiguously. Ideal bond and angle parameters for the TPI molecule were

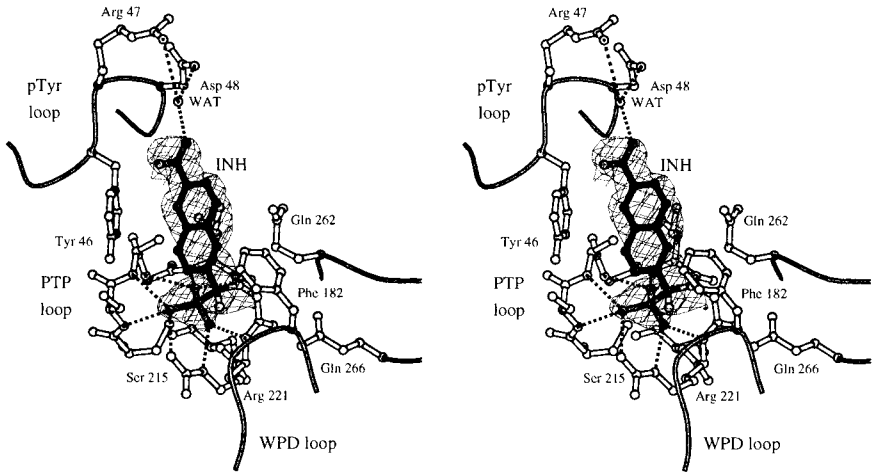

FIGURE 2: Stereoview of the $2F_o - F_c$ simulated annealing OMIT electron density map of the INH inhibitor bound to PTP1B, contoured at 1.0 sigma. All figures were prepared using MOLSCRIPT (*38*).

Table 1: Crystallographic Data and Refinement Statistics[a]

inhibitor	TPI	FOMT	INH
	Crystal Parameters		
space group	$P3_121$	$P2_1$	$P3_121$
a (Å)	88.5	39.7	88.3
b (Å)	88.5	86.8	88.3
c (Å)	104.6	52.0	104.6
α (deg)	90.0	90.0	90.0
β (deg)	90.0	96.91	90.0
γ (deg)	120.0	90.0	120.0
Z	1	1	1
	Data Collection Parameters		
resolution limits (Å)	14−2.35	8−2.10	8−2.25
crystals (*N*)	1	1	1
measurements (*N*)	65906	46108	84763
unique reflections	18772	15934	22196
completeness (%)	94.4 (93.8)[b]	78.1 (55.7)[b]	97.0 (76.2)[b]
R_{sym} (%)[c]	3.3 (8.9)[b]	2.9 (7.4)[b]	5.6 (26.5)[b]
R_{meas} (%)[d]	3.9 (10.6)[b]	3.4 (9.7)[b]	4.7 (24.2)[b]
mean $I/\sigma(I)$	16.8 (8.2)[b]	13.7 (8.8)[b]	15.6 (7.8)[b]
X-ray source	rotating anode	ELETTRA	rotating anode
λ (Å)	1.541	1.0	1.541
	Refinement Parameters*		
protein and ligand atoms (*N*)	2456	2495	2394
water molecules (*N*)	157	88	236
R factor (%)[e]	20.4 (25.3)[b]	21.1 (31.0)[b]	20.8 (29.0)[b]
free *R* factor (%)	25.6 (27.8)	26.2 (33.6)	
rmsd bond lengths (Å)	0.006	0.009	0.011
rmsd bond angles (deg)	1.392	1.625	1.380
reflections used (*N*)	18704	14569	20471

[a] All recorded reflections were used during maximum likelihood refinement in REFMAC. The quoted *R* factors were calculated using all data. [b] Numbers in brackets refer to the values in the highest-resolution shell; 2.48−2.35 Å for the PTP1B−TPI inhibitor complex data, 2.21−2.1 Å for the PTP1B−FOMT peptide inhibitor complex data and 2.35−2.25 Å for the PTP1B−INH inhibitor complex data. [c] $R_{sym} = \sum_h \sum_i |I(h) - I_i(h)|/\sum_h \sum_i I_i(h)$, where $I_i(h)$ and $I(h)$ are the *i*th and mean measurements of the intensity of reflection *h*. [d] R_{meas} is the multiplicity weighted R_{sym} (*39*). [e] *R* factor $= \sum_h |F_o - F_c|/\sum_h F_o$, where F_o and F_c are the observed and calculated structure factors amplitudes of reflection *h*. *λ*: wavelength. rmsd: root mean square deviation. *Z*: The number of molecules in the crystallographic asymmetric unit.

calculated using SYBYL (*28*). Refinement with X-PLOR (*26*), using simulated annealing and torsional dynamic algorithms, was alternated with model building within O (*29*). Water molecules present in the crystal structure were identified using ARP (*30*) resulting in a final model with an *R* factor of 0.204 and a free *R* factor of 0.256 for data in the resolution range 14−2.3 Å (Table 1). In Figure 3, a portion of the simulated annealing $2F_o - F_c$ OMIT map in the vicinity of the catalytic site indicates that all atoms of the inhibitor are placed within density.

PTP1B−FOMT Peptide Complex. Structure determination of the PTP1B−FOMT peptide complex, which crystallized in a different space group from the native apo-PTP1B enzyme, was achieved with molecular replacement using the native apo-PTP1B coordinates as a search model. Electron density in the initial difference Fourier map was sufficient to place the fluoromalonyl tyrosine and the leucine ($P + 1$) residues, although density for the remainder of the FOMT molecule was less well-resolved. Subsequent refinement of the protein structure alone with cycles of REFMAC (*31*), utilizing maximum likelihood theory, and ARP (*30*) improved the phasing sufficiently for portions of the inhibitor to be assigned to density. Further rounds of phasing and refinement using REFMAC and ARP resulted in a final model with an *R* factor of 0.211 and a free *R* factor of 0.262 (Table 1) for data in the resolution range 8−2.1 Å. Ideal bond and angle parameters for the FOMT molecule were also obtained using SYBYL (*28*). The $2F_o - F_c$ electron map in the vicinity of the catalytic site is shown in Figure 5.

RESULTS

Structure of the PTP1B−INH Complex. The overall structure of the PTP1B−INH complex is virtually identical to that of the PTP1B−[1,1-difluro-1-(naphth-2-yl)]methylphosphonic acid (NAPTH) complex reported previously (Figure 2) (*18*); the two structures superimpose such that equivalent protein Cα atoms deviate within an rmsd of 0.22 Å. The three terminal oxygen atoms of the inhibitor phosphonate moiety accept a total of 8 hydrogen bonds from main-chain amide groups of the PTP signature motif residues and the Arg 221 guanidinium side chain. The inhibitor naphthalene ring forms hydrophobic interactions with the phenyl rings of Tyr 46 of the pTyr recognition loop and Phe 182 of the WPD loop which adopts the catalytically competent closed conformation. Interactions between the Phe 182 phenyl ring and the inhibitor are augmented by van der Waals interactions with the two fluorine atoms of the

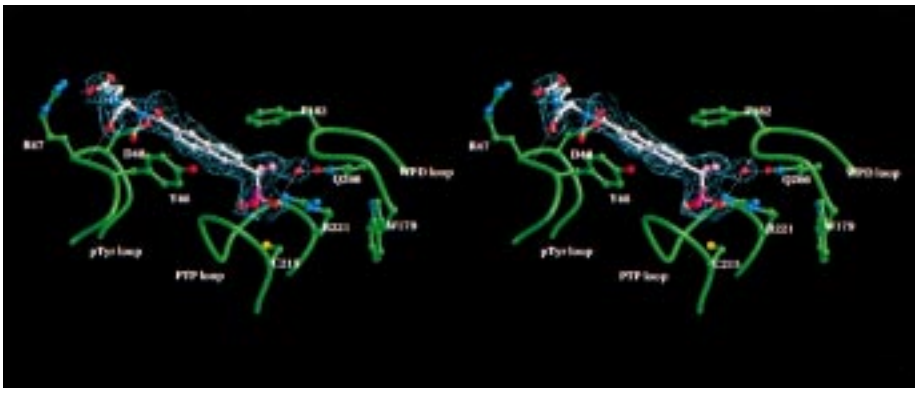

FIGURE 3: Stereoview of the $2F_o - F_c$ simulated annealing OMIT electron density map of the TPI inhibitor bound to PTP1B, contoured at 1.0 sigma.

diflurophosphonate group. The carboxylate group of the inhibitor results in the formation of additional protein−inhibitor interactions compared with those of the PTP1B−NAPTH complex. These involve interactions between the side chains of Arg 47 and Asp 48 and the inhibitor−carboxylate group that are mediated via an enzyme-bound water molecule (Figure 2).

Structure of the PTP1B−TPI Complex. Electron density OMIT maps reveal clearly resolved electron density corresponding to the TPI molecule bound to the PTP1B catalytic site with the WPD loop in the closed conformation, similar to that for the other [1,1-difluoro-1-(naphth-2-yl)]methylphosphonic acid-containing molecules (Figures 3, 4). However, the peptide mimetic portion of TPI provides additional scope for protein−inhibitor interactions and forces a change in the orientation of the naphthalene ring of TPI at the PTP1B catalytic site relative to that of other [1,1-difluoro-1-(naphth-2-yl)]methylphosphonic inhibitors.

Mode of Binding of the [1,1-Difluoro-1-(naphth-2-yl)]-methylphosphonate Moiety. As a result of rigid body rotation of the inhibitor by 30°, the position of the naphthalene ring is displaced relative to the naphthalene rings of the other [1,1-difluoro-1-(naphth-2-yl)]methylphosphonic inhibitors (Figure 5). However, the naphthalene ring forms similar contacts with catalytic site residues, and there are no changes in the side-chain conformations of the catalytic site residues. In all three PTP1B−inhibitor complexes, the phenyl ring of Phe 182 interacts more closely with the naphthalene ring than with the phenyl ring of pTyr in the PTP1B−pTyr peptide complex, rotating by ~90° around its Cβ−Cγ bond. A similar conformation in the PTP1B−pTyr peptide complex would result in a short contact (2.8 Å) between the aromatic ring of Phe 182 and the carbonyl oxygen of pTyr. Motion of the naphthalene ring of TPI relative to that of other PTP1B [1,1-difluoro-1-(naphth-2-yl)]methylphosphonic inhibitors provides a binding cavity for an enzyme-bound water molecule (WAT 12) that links the main-chain nitrogen atom of Phe 182 and amide side chain of Gln 266 of PTP1B with a terminal phosphate oxygen atom and the *Pro-S* fluorine atom of the inhibitor (Figures 3, 4). A similar water molecule is observed in the PTP1B−pTyr peptide complex (*15*).

Mode of Binding of the Peptide Mimetic Moiety. The carboxamidoglutamic acid portion of TPI forms several main-chain hydrogen bond interactions with PTP1B, resembling those observed in the PTP1B−pTyr peptide complex (*15*). The carboxamido-N1-atom of the inhibitor, equivalent to the main-chain nitrogen atom of pTyr of the PTP1B−pTyr hexapeptide complex, donates a hydrogen bond to the carboxylate side chain of Asp 48 (Figures 3, 4). In addition, the main-chain amide nitrogen of Arg 47 donates a hydrogen bond to the carbonyl oxygen atom of the terminal amide moiety of the inhibitor, equivalent to that observed between Arg 47 and Asp (P-2) of the phosphotyrosine hexapeptide in the PTP1B−pTyr hexapeptide complex (*15*). These interactions are conserved as a result of the ~1 Å motions of the Arg 47 and Asp 48 residues between the two structures. The glutamate residue of TPI, which was predicted to form a salt-bridge interaction with the Arg 47 side chain similar to that observed between Arg 47 and the peptide Glu (P-1) residue in the PTP1B−pTyr peptide complex (22), is situated ~4 Å from the guanidinium group of Arg 47, with the aliphatic portion packing against the aliphatic portion of Asp 48 (C−C distance 3.7 Å). This unusual interaction is further stabilized by the hydrogen bond between the N1 atom of the TPI inhibitor and the side chain of Asp 48. It should be noted that the Glu (P-1)-Arg 47 is a long hydrogen bond in the PTP1B−pTyr peptide complex (3.2 Å) (ref *15*) and that the side chain of the glutamate residue of TPI forms a hydrogen bond with a well-defined water molecule, potentially compensating for the lack of interaction with Arg 47.

Structure of the PTP1B−FOMT Cyclic Peptide Complex. Residues of the cyclic FOMT peptide are well-resolved within the $2F_o - F_c$ electron density map (Figure 6). As reflected in the relative *B* factors of the inhibitor residues, the Asp(P-4) and Ala(P-3) residues are less well-ordered than the FOMT residue. In all instances, the *B* factors of the FOMT peptide residues are higher than the protein residues with which they interact (Table 2). The FOMT residue binds to PTP1B with the Arg 221 side chain and WPD loop adopting the open conformation, characteristic of the unliganded state of PTP1B (*14*) (Figures 7, 8). In all previously determined substrate and inhibitor complexes, with the exception of a PTP1B−tungstate complex, the WPD loop adopts the closed position, accompanied by a conformational change of the Arg 221 side chain.

The Phosphate Mimetic (Malonyl Group) of the FOMT Residue. The differences in structures between the malonyl group of FOMT and the phosphate group of a pTyr residue are reflected in differences in the hydrogen bonding patterns between the phosphate and malonyl groups bound to the PTP1B catalytic site. The two oxygen atoms of one of the carboxylate groups are equivalent in position to within 0.3

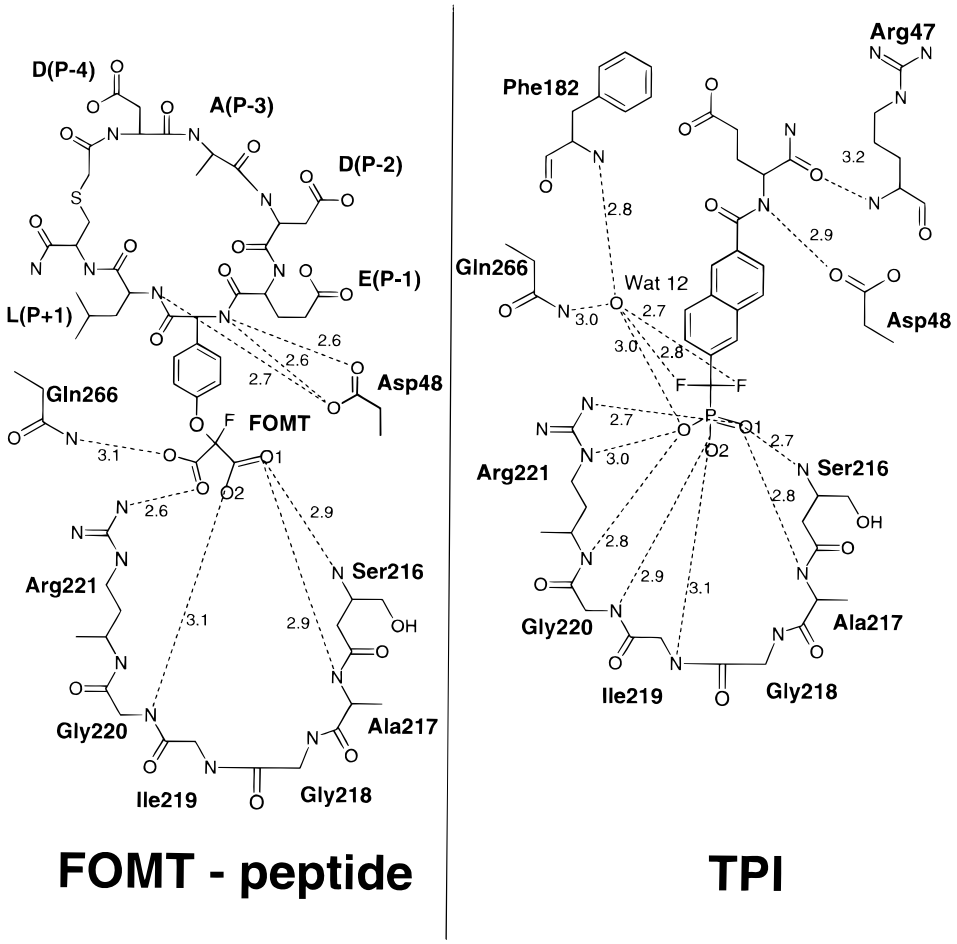

FIGURE 4: Schematic of TPI and FOMT peptide−PTP1B interactions. Hydrogen bonds are indicated as dashed lines. A distance criterion of 3.2 Å was used.

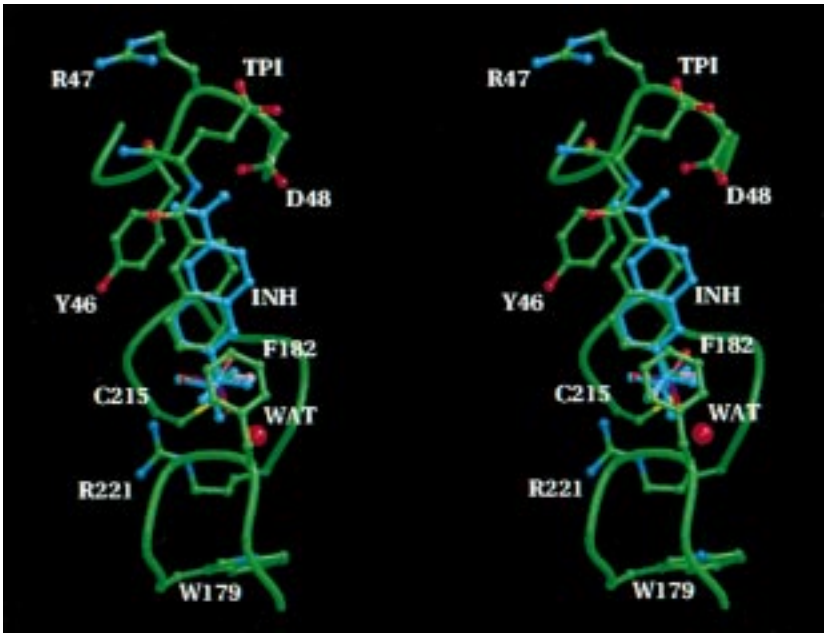

FIGURE 5: Stereoview showing the superimposition the INH molecule (cyan) onto the PTP1−TPI inhibitor complex at the PTP1B catalytic site. The protein coordinates (Cα atoms) of the PTP1B−TPI complex were superimposed onto the equivalent atoms of the PTP1B−INH complex.

Å of two of the oxygen atoms of the phosphonate moiety of TPI at the PTP1B catalytic site (Figure 9, labeled O1 and O2). For all phosphoryl ligands bound to the catalytic site of PTP1B, these two latter oxygen atoms accept hydrogen bonds from the amide nitrogens of Ser 216, Ala 217, and Ile 219, and following a conformational change of the Arg 221 guanidinium side chain, the NH2-atom of Arg 221 (Figure 4). In the PTP1B−FOMT peptide complex, however,

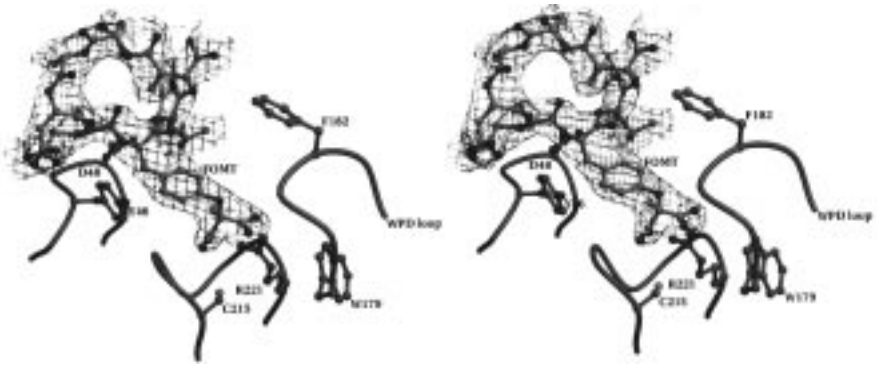

FIGURE 6: $2F_o - F_c$ electron density map, contoured at 1.0 sigma, of the FOMT cyclic peptide inhibitor bound to PTP1B.

Table 2: Average Group Temperature Factors for Main-Chain and Side-Chain Groups of the FOMT Peptide Inhibitor and Protein Residues of the Surrounding Binding Site of the PTP1B−FOMT Peptide Complex

FOMT peptide group	*B* factors (Å^2) main chain	side chain
FOMT (malonyl group)		70
FOMT (phenyl ring)	74	68
Leu ($P + 1$)	75	85
Glu ($P - 1$)	73	85
Asp ($P - 2$)	83	85
Ala ($P - 3$)	83	84
Asp ($P - 4$)	90	92
PTP1B		
PTyr loop		
Tyr 46	58	62
Arg 47	61	70
Asp 48	61	63
Val 49	54	57
WPD loop		
Trp 179	59	69
Por 180	70	70
Asp 181	72	72
Phe 182	71	66
PTP loop		
Cys 215	55	55
Ser 216	55	58
Ala 216	46	
Gly 218	50	49
Ile 219	54	
Gly 220	52	65
Arg 221		

the slight difference in position of the two oxygen atoms of the carboxylate group of the malonyl residue results in fewer hydrogen bonds to the enzyme that comprise hydrogen bonds with the amide group of Ser 216, Ala 217, and Gly 220 (Figure 4). The apostate conformation of the Arg 221 side chain results in a loss of the hydrogen bond between the O1-atom of FOMT and the NH2 atom of Arg 221 (Figures 4, 9). The oxygen atoms of the second carboxylate group of the malonyl moiety are not equivalent to any of the phosphate oxygen atoms of a pTyr residue or the TPI molecule (Figure 9). This group forms a hydrogen bond with the more highly charged NH1 atom of Arg 221, rather than the NE atom. This second carboxylate group occupies a position similar to that of a highly ordered water molecule observed in the PTP1B−pTyr peptide and PTP1B−TPI (WAT 12) complex structures. The fluorine atom of the FOMT is over 4 Å away from a neighboring water molecule or protein atom; however, its position would be 3.5 Å from the carboxylate group of Asp 181 if the WPD loop were in the closed conformation (Figure 10).

The Phenyl Ring Moiety of the FOMT Residue. The aromatic ring of the FOMT peptide inhibitor is bound to the

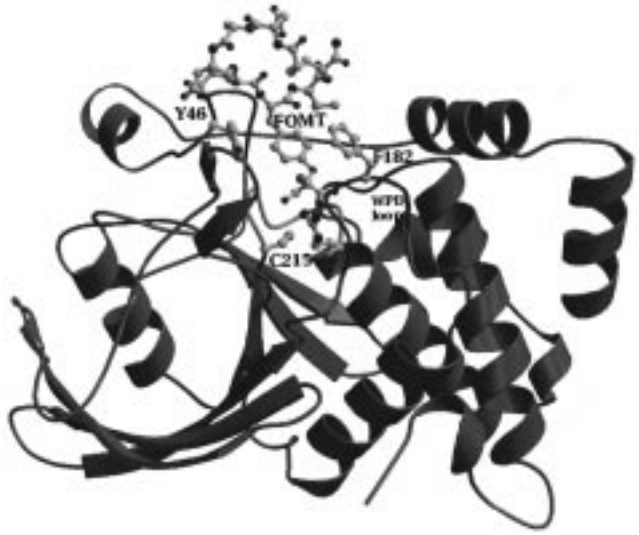

FIGURE 7: Ribbons diagram of the PTP1B−FOMT peptide complex. The FOMT peptide, Tyr 46, Phe 182, Cys 215, and Arg 221 residues of PTP1B are represented as ball-and-stick.

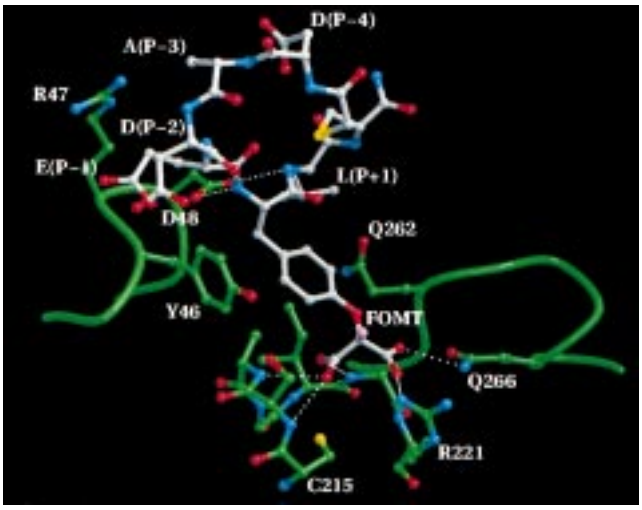

FIGURE 8: View of the interactions between the FOMT peptide inhibitor and the catalytic site of PTP1B.

hydrophobic pocket of the catalytic site in a manner similar to that of the phenyl ring of pTyr in the PTP1B−pTyr peptide complex (Figure 10). The FOMT phosphate-mimicking moiety is larger than the phosphate of the pTyr residue in the PTP1B−pTyr peptide complex. As a consequence, the phenyl ring of FOMT is displaced 1.4 Å away from the PTP motif residues compared with the equivalent moiety in the

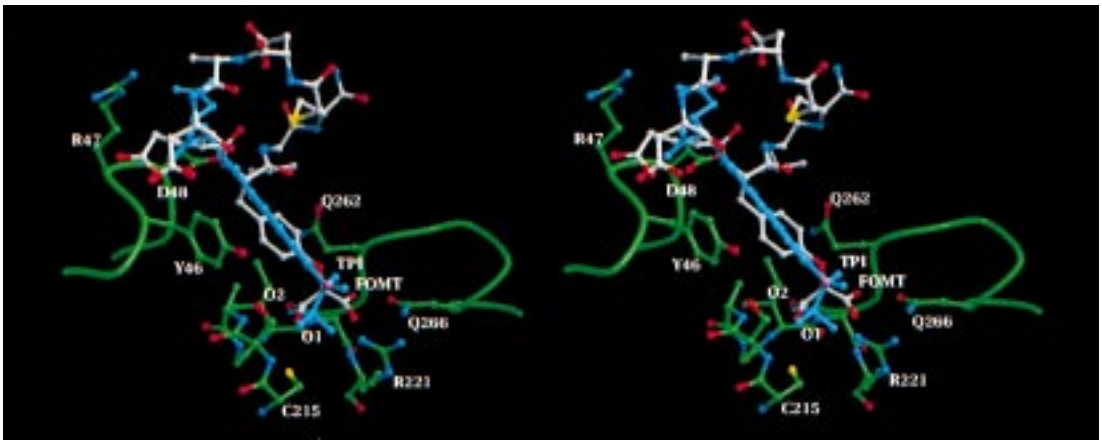

FIGURE 9: Superimposition the TPI molecule (cyan) onto the PTP1B−FOMT peptide inhibitor complex at the PTP1B catalytic site. The protein coordinates (Cα atoms) of the PTP1B−TPI complex were superimposed onto the equivalent atoms of the PTP1B−FOMT complex.

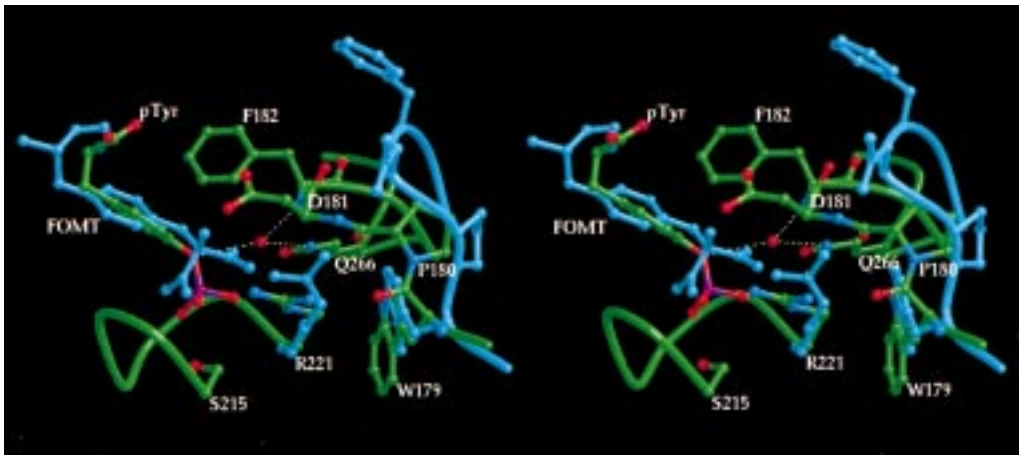

FIGURE 10: Details of the difference in conformation of the WPD loop in the PTP1B−pTyr peptide complex (atom colors) and the PTP1B−FOMT complex (cyan). Only the pTyr and FOMT residues of the protein ligands are shown. The protein coordinates (Cα atoms) of the PTP1B−pTyr complex were superimposed onto the equivalent atoms of the PTP1B−FOMT complex.

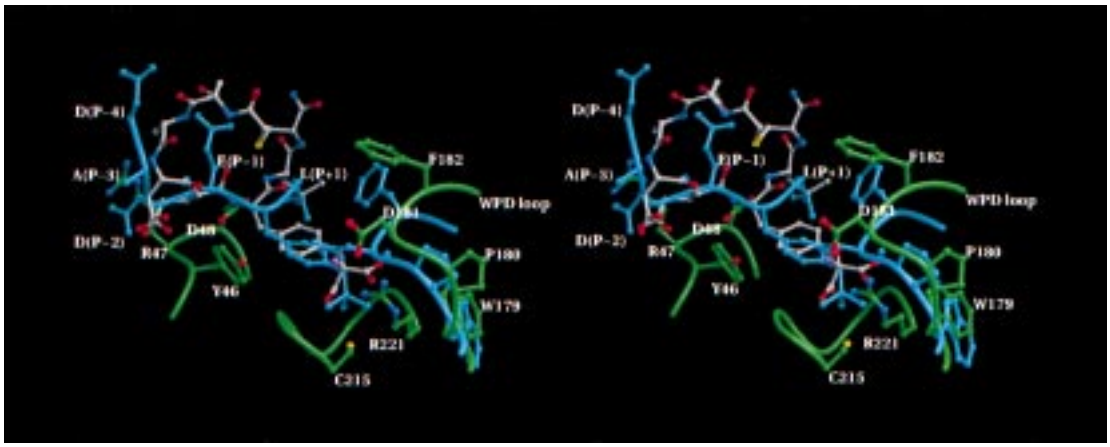

FIGURE 11: Superimposition of D-A-D-E-pY-L peptide and WPD loop (cyan) (*15*) onto the PTP1B−FOMT peptide inhibitor complex at the PTP1B catalytic site. The residues of the D-A-D-E-pY-L peptide are labeled. The protein coordinates (Cα atoms) of the PTP1B−pTyr complex were superimposed onto the equivalent atoms of the PTP1B−FOMT complex.

PTP1B−pTyr peptide complex (Figure 11). Hydrophobic packing interactions are conserved between the phenyl ring of FOMT and the side chains of Tyr 46, Val 49, Ala 217, Ile 219, and the aliphatic portion of Gln 262, with those observed in the PTP1B−pTyr complex; however the open conformation of the WPD loop results in a loss of the hydrophobic stacking interactions with the phenyl ring of Phe 182.

Peptide Mimetic. The FOMT and Leu (P + 1) residues of the cyclic FOMT peptide inhibitor correspond closely with equivalent residues of the D-A-D-E-pY-L peptide of the PTP1B−pTyr peptide complex (*15*) (Figure 11). Within both complexes, the carboxylate side chain of Asp 48 accepts hydrogen bonds from the main-chain amide groups of the pTyr (or FOMT) and Leu (*P* + 1) residues (Figures 4, 8). The side chain of Leu (P + 1) occupies a shallow

hydrophobic pocket and packs against the side chains of Val 49, Ile 219, and Met 258, although it does not completely fill this pocket. Residues N-terminal of the FOMT residue in the cyclic peptide occupy different positions relative to their counterparts in the PTP1B-pTyr peptide complex. Despite these differences, a long salt bridge (3.5 Å) is observed between the side chain of Glu ($P - 1$) of the FOMT peptide with the side chain of Arg 47 that is similar to the salt bridge observed within the PTP1B−pTyr peptide complex (Figures 4, 8, 11). To accommodate the differences in the position of the Glu ($P - 1$) residue between the two complexes, the side chain of Arg 47 adopts two distinct conformations. In the PTP1B−pTyr peptide complex, the main-chain amide group of Arg 47 donates a hydrogen bond to the carbonyl oxygen atom of Asp ($P - 3$); however this hydrogen bond is not present within the PTP1B−FOMT inhibitor complex. The remainder of the FOMT inhibitor protrudes into the solvent region of the crystal, and an equivalent salt bridge to that observed between the side chains of Arg 47 of PTP1B and peptide Asp ($P - 2$) residue of the PTP1B−pTyr peptide complex is not formed in the PTP1B−FOMT peptide complex.

DISCUSSION

[1,1-Difluoro-1-(naphth-2-yl)]methylphosphonate-Based Inhibitor Interactions. The structures of the difluorophosphonate-containing INH and TPI inhibitors complexed to PTP1B reveal that attachment of functional groups to the naphthalene ring affords the scope for additional inhibitor−protein interactions involving phosphatase residues that are remote from the catalytic site. Such interactions serve to increase the affinity of PTP1B−inhibitor complexes and, since PTP sequence variations occur within these residues, allow the development of specific PTP inhibitors. Iterative cycles of crystal structure determination and rationale drug design that result in functional groups mimicking interactions between PTP1B and a peptide substrate have the potential to yield improved inhibitors with enhanced affinity and specificity. One limitation of phosphonate-based inhibitors, however, is that the high charge of the phosphonate group restricts cellular penetration, which probably reduces their potential as in vivo therapeutic agents. The problem of cell membrane penetration associated with the phosphonate-based pTyr mimetics has been addressed by the development of the non-phosphorus fluoromalonyl tyrosine residues.

FOMT Cyclic Peptide. Although the FOMT residue in the cyclic peptide inhibitor binds to the pTyr-binding site of the catalytic site, unlike complexes of PTP1B with pTyr residues in peptides and [1,1-difluoro-1-(naph-2-yl)]methylphosphonic acid groups, the WPD loop and Arg 221 side chain adopt the open conformation, typical of the ligand-free state of PTP1B.

The reasons why the WPD loop remains open in the PTP1B−FOMT cyclic peptide inhibitor complex are probably 2-fold and result from the differences in structures between a malonyl group and a phosphate group, and the concerted motions of the Arg 221 side chain and WPD loop. In the PTP1B−pTyr and PTP1B−difluoronaphthymethyl phosphonate complexes, motions of the Arg 221 side chain and closure of the WPD loop are stabilized (i) by bidentate interactions between the guanidinium group of Arg 221 and two phosphate/phosphonate oxygen atoms and (ii) by a buried water molecule that links the amide nitrogen atom of Phe 181 with the side chain of Gln 266 and either a phenolic oxygen atom (pTyr) or a fluorine atom (TPI). The concerted motion of the Arg 221 side chain and WPD loop results from hydrophobic packing between the aliphatic moiety of Arg 221 and Trp 179 side chain, in both open and closed states, and the hydrogen bond between the guanidinium NH1 atom of Arg 221 with the carbonyl oxygen atom of Pro 180 in the closed state. Similar conformational changes of the equivalent Arg residue and WPD loop were observed in the *Yersinia* PTP in complexes with tungstate and sulfate (*32*, *33*). Molecular modeling indicates that the position of the guanidinium group of Arg 221 in the apostate is too remote from the ligand phosphate oxygen atoms to form hydrogen bonds. The Arg 221 side chain does not undergo a conformational change in the presence of an FOMT residue for numerous reasons. One is that, in the apostate conformation, a strong hydrogen bond (2.6 Å) is formed between the NH1 atom of Arg 221 and a carboxylate oxygen atom of FOMT which would be lost were Arg 221 to undergo a conformational change. Second, because of differences in positions between the three terminal oxygen atoms of a phosphate group and the four oxygen atoms of the malonyl group, an Arg 221 side chain with the closed conformation would not form suitable hydrogen bonds with carboxylate groups of the malonyl derivative. These two factors suggest that an Arg 221 side chain in the closed conformation would form less favorable interactions with the malonyl moiety than an Arg residue that adopts the open conformation. The second reason for the open conformation of the WPD loop results from the finding that one of the malonyl carboxylate groups occupies a site close to that of the buried water molecule observed in the PTP1B−pTyr peptide and PTP1B−TPI complexes. Although the carboxylate group of the FOMT residue forms a compensatory hydrogen bond to Gln 266, that to the main-chain nitrogen of Phe 182 is not compensated (3.6 Å). Hence, closure of the WPD loop would create a cavity in the vicinity of the Phe 182 main chain and an uncompensated main-chain nitrogen atom.

Similarly to the [1,1-difluoro-1-(naphth-2-yl)]methylphosphonic acid derivatives, peptidic functional groups attached to the FOMT residue form interactions with PTP1B residues that flank the catalytic site, providing a mechanism to introduce PTP specificity and to enhance potency. The hydrogen bond between the carboxylate side chain of Asp 48 and main-chain nitrogen of the pTyr, or pTyr mimetic, is a conserved feature of PTP1B−pTyr mimetic inhibitor complexes. This interaction is likely to be important in determining the orientation of the substrate/inhibitor across the relatively flat surface of PTP1B external to the catalytic site pocket. In both the PTP1B−pTyr peptide and the PTP1B−TPI and FOMT peptide complexes, the Arg 47 side chain interacts with the carboxylate groups of the ligand, potentially conferring selectivity for inhibitors with negative groups adjacent to the pTyr mimetic. The size of the hydrophobic pocket of PTP1B which recognizes the Leu ($P + 1$) side chain, suggests that more bulky hydrophobic groups on the inhibitor would contribute additional inhibitor−protein interactions by improvements in hydrophobic packing. Interestingly, Maclean et al. showed previously that

a Leu to Ala substitution at this site within phosphotyrosine peptides significantly reduces binding affinity (*34*). This site on PTP1B is equivalent to that of an aryl-phosphate-binding site in PTP1B reported by Puius et al., 1997 (*35*).

A number of structural features determine PTP1B inhibitor affinities, for example the presence of a fluorine atom on the FOMT residue and the cyclic or linear property of the peptides. The cyclic peptide inhibitors are significantly more potent than their linear peptide equivalents (*20*−*22*) (Figure 1). Potentially, the loss of entropy of the inhibitor upon binding to PTP1B is less for the cyclic peptide inhibitors than for the linear peptides, providing an enhancement of binding affinity. The linear FOMT peptide inhibitor exhibits a 10-fold higher K_i than that of the linear OMT inhibitor (K_i of 1 and 13 μM, respectively), (*20*) although for the cyclic inhibitors, the presence of the fluorine atom enhances affinity to a lesser extent (*22*) (Figure 1). The PTP1B−FOMT cyclic peptide complex structure indicates that the fluorine atom does not form strong interactions with either protein or water atoms. The only atom within 4 Å is a water molecule that is hydrogen bonded to Lys 120. The effect of the fluorine atom of the FOMT may be to stabilize this hydrogen bond and concurrently stabilize Lys 120. The fluorine atom may also play an indirect role to enhance affinity, resulting from the reduced pK_a of the carboxylic acid groups of the OMT residue of 1.1 pH units (*21*), hence increasing the negative charge density of this group, more similar to that of a phosphate group. This would be consistent with the finding that both carboxylate groups of the OMT residue are essential for high-affinity PTP1B interactions. Removal of one of the carboxylate groups from the OMT residue causes a dramatic 500-fold reduction in affinity of the resulting compound (*23*) (Figure 1). The single carboxylate possessed by A (Figure 1) could adopt either of the two positions displayed by the two carboxylate groups of the FOMT moiety, although it is most likely to resemble the carboxylate with more interactions with the PTP loop. In the PTP1B−FOMT peptide complex we observed that the carboxylate which more closely mimics two of the oxygen atoms of the phosphate of the pTyr in the PTP1B−pTyr peptide complex may form hydrogen bonds to the amide nitrogens of Ser 216, Ala 217, and Gly 220. The second carboxylate of the FOMT residue forms hydrogen bonds with the amide side chain of Gln 266 and the NH1 atom of Arg 221. The additional carboxylate on the phenol ring of inhibitor B improves the affinity (*23*) (Figure 1). This carboxylate can be modeled on two sides of the phenolic ring of FOMT. On one side it would potentially clash against Tyr 46, but on the other it could potentially form a hydrogen bond with the side chain of Gln 266.

The structure of the PTP1B−FOMT peptide complex presented here provides a basis for understanding the mechanisms by which a malonyl−tyrosine group mimics PTP1B−phosphotyrosine interactions, and these findings may also be applicable to an understanding of malonyl−tyrosine peptide interactions with SH2 domains. As a consequence of the more bulky character of a malonyl moiety compared with a phosphate group, a malonyl−tyrosine residue forms fewer interactions with PTP1B than a phosphotyrosine residue. These reduced interactions include fewer hydrogen bonds to residues of the PTP motif (Cys 215 to Arg 221) and, as a result of the open conformation of the WPD loop, loss of hydrophobic interactions between the phenyl ring of the malonyl−tyrosine residue and Phe 182 of the WPD loop. These structural results are consistent with the 10-fold greater affinity of the D-A-D-E-pY-L peptide toward PTP1B where the pTyr residue is replaced with a difluorophosphonomethyl phenylalanine residue rather than by a fluoromalonyl−tyrosine residue (*16*, *22*). The structure of the PTP1B−FOMT complex reported here is the first crystal structure of non-phosphonate-containing inhibitor bound to a protein tyrosine phosphatase. The structure reveals that ligand binding to PTP1B is possible without inducing closure of the catalytic site WPD loop. This structure and that of the PTP1B−INH and PTP1B−TPI complexes indicate that ligand substitutions affect protein−ligand affinities directly by promoting novel protein−ligand interactions and also indirectly, as observed for the fluorine substituent of FOMT, by perturbing the pK_a of the carboxylate group of the malonyl moiety of the FOMT residue.

REFERENCES

1. Neel, B. G., and Tonks, N. K. (1997) *Curr. Opin. Cell Biol. 9*, 193−204.
2. Denu, J. M., Stuckey, J. A., Saper, M. A., and Dixon, J. E. (1996) *Cell 87*, 361−364.
3. Fauman, E. B., and Saper, M. J. (1996) *Trends Biochem. Sci. 21*, 413−417.
4. Frangioni, J. V., Beahm, P. H., Shifrin, V., Jost, C. A., and Neel, B. G. (1992) *Cell 68*, 545−560.
5. Sugimoto, S., Wandless, T., Shoelson, S. E., Neel, B. G., and Walsh, C. T. (1994) *J. Biol. Chem. 269*, 13614−13622.
6. Barford, D., and Neel, B. G. (1998) *Structure 6*, 249−254.
7. Schultz, L. D., Schweitzer, P. A., Rajan, T. V., Yi, T., Ihle, J. N., Matthews, R. J., Thomas, M. L., and Beier, D. R. (1993) *Cell 73*, 1445−1454.
8. Li., J., Yen, C., Liaw, D., Podsypanina, K., Bose, S., Wang, S. I., Puc, J., Miliaresis, C., Rodgers, L., McCombie, R., Bigner, S. H., Giovanella, B. C., Ittmann, M., Tycko, B., Hibshoosh, H., Wigler, M. H., and Parsons, R. (1997) *Science 275*, 1943−1947
9. Steck, P. A., Pershouse, M. A., Jasser, S. A., Yung, W. K., Lin, H., Ligon, A. H., Langford, L. A., Baumgard, M. L., Hattier, T., Davies, T., Frye, C., Hu, R., Swedlund, B., Teng, D. H., and Tavtigian, S. V. (1997) *Nat. Genet. 15*, 356−362.
10. Tamura, M., Gu, J., Matsumoto, K., Aota, S., Parsons, R., and Yamada, K. M. (1998) *Science 280*, 1614−1617.
11. Seely, B. L., Staubs, P. A., Reichart, D. R., Berhanu, P., Milarski, K. L., Saltiel, A. R., Kusari, J., and Olefsky, J. M. (1996) *Diabetes 45*, 1479−1385.
12. Ahmad, F., Li, P. M., Meyerovitch, J., and Goldstein, B. J. (1995) *J. Biol. Chem. 270*, 20503−20508.
13. Burke, T. R., Jr., and Zhang, Z. Y. (1998) *Pept. Sci. 47*, 225−241.
14. Barford, D., Flint, A. J., and Tonks, N. K. (1994) *Science 263*, 1397−1404.
15. Jia, Z., Barford, D., Flint. A. J., and Tonks, N. K. (1995) *Science 268*, 1754−1758.
16. Burke, T. R., Jr., Kole H. K., and Roller, P. P. (1994) *Biochem. Biophys. Res. Commun. 204*, 129−134.
17. Kole, H. K., Smyth, M. S., Russ, P. L., and Burke, T. R., Jr. (1995) *Biochem. J. 311*, 1025−1031.
18. Burke, T. R., Ye, B., Yan, X., Wang, S., Jia, Z., Chen, L., Zhang, Z.-Y., and Barford, D. (1996) *Biochemistry 35*, 15989−15996.
19. Kole, H. K., Akamatsu, M., Ye, B., Yan, X., Barford, D., Roller, P. R., and Burke, T. R., Jr. (1995) *Biochem. Biophys. Res. Commun. 209*, 817−822.
20. Akamatsu, M., Roller, P. P., Chen, L., Zhang, Z. Y., Ye, B., and Burke, T. R., Jr. (1997) *Bioorg. Med. Chem. 5*, 157−163.

21. Burke, T. R., Jr., Ye, B., Akamatsu, M., Ford, H., Jr., Yan, X. Y., Kole, H., Wolf, G., Shoelson, S. E., and Roller, P. P. (1996) *J. Med. Chem. 39*, 1021−1027.
22. Roller, P. P., Wu, L., Zhang, Z.-Y., and Burke, T. R., Jr. (1998) *Bioorg. Med. Chem. Lett. 8*, 2149−2150.
23. Yao, Z. J., Ye, B., Wu, X. W., Wang, S., Wu, L., Zhang, Z. Y., and Burke, T. R., Jr. *Bioorg. Med. Chem*. (in press).
24. Barford, D., Keller, J. C., Flint, A. J., and Tonks, N. K. (1994) *J. Mol. Biol*. *239*, 726−730.
25. Otwinoski, Z., and Minor, W. (1997) Processing X-ray diffraction data collected in oscillation mode, in *Methods Enzymology* (Carter, C., and Sweet, B., Eds.) Vol. 277, pp 307−326, Academic Press, New York.
26. Brunger, A. T. (1992) X-PLOR: version 3.1. Yale University Press, New Haven, CT.
27. Navaza, J. (1994) *Acta Crystallogr., Sect. A 50*, 157−160.
28. SYBYL 6.4 Tripos Inc., 1699 South Hanley Road, St. Louis, Missouri, 63144.
29. Jones, T. A., Zou, J. Y., Cowan, S. W., and Kjeldgaard, M. (1991) *Acta Crystallogr., Sect. A 47*, 110−119.
30. Lamzin, V. S., and Wilson, K. S. (1997) *Methods Enzymology* (Carter, C., and Sweet, B. Eds.) Vol. 277, pp 269−305, Academic Press, New York.
31. Murshudov, G. N., Vagin, A. A., and Dodson, E. J. (1997) *Acta Crystallogr., Sect. D 53*, 240−255.
32. Stuckey, J. A., Schubert, H. L., Fauman, E. B., Zhang, Z. Y., Dixon, J. E., and Saper, M. A. (1994) *Nature 370*, 571−575.
33. Schubert, H. L., Fauman, E. B., Stuckey, J. A., Dixon, J. E., and Saper, M. A. (1995) *Protein Sci. 4*, 1904−1913.
34. Maclean, D., Sefler, A. M., Zhu, G., Decker, S. J., Salteil, A. R., Singh, J., McNamara, D. M., Dobrusin, E. M., and Sawyer, T. K. (1995) *Protein Sci. 4*, 13−20.
35. Puius, Y. A., Zhao, Y., Sullivan, M., Lawrence, D. S., Almo, S. C., and Zhang, Z.-Y. (1997) *Proc. Natl. Acad. Sci. U.S.A. 94*, 13420−13425.
36. Zhang, Z. Y., Maclean, D., McNamara, D. J., Sawyer, T. K., and Dixon, J. E. (1994) *Biochemistry 33*, 2285−2290.
37. Burke, T. R., Jr., Yao, Z. J., Zhao, H., Milne, G. W. A., Wu, L., Zhang, Z.-Y., and Voigt, J. H. (1998) *Tetrahedron 54*, 9981−9994.
38. Kraulis, P. (1991) *J. Appl. Crystallogr*. *24*, 946−950.
39. Diederichs, K., and Karplus, A. P. (1997) *Nat. Struct. Biol. 4*, 269−275.

BI9816958